nature neuroscience

A subcortical inhibitory signal for behavioral arrest in the thalamus

Kristóf Giber[1,11], Marco A Diana[2–4,11], Viktor M Plattner[1,11], Guillaume P Dugué[2–4], Hajnalka Bokor[1], Charly V Rousseau[2–4], Zsófia Maglóczky[5], László Havas[6,7], Balázs Hangya[5,8], Hendrik Wildner[9], Hanns Ulrich Zeilhofer[9,10], Stéphane Dieudonné[2–4] & László Acsády[1]

Organization of behavior requires rapid coordination of brainstem and forebrain activity. The exact mechanisms of effective communication between these regions are presently unclear. The intralaminar thalamic nuclei (IL) probably serves as a central hub in this circuit by connecting the critical brainstem and forebrain areas. We found that GABAergic and glycinergic fibers ascending from the pontine reticular formation (PRF) of the brainstem evoked fast and reliable inhibition in the IL via large, multisynaptic terminals. This inhibition was fine-tuned through heterogeneous GABAergic and glycinergic receptor ratios expressed at individual synapses. Optogenetic activation of PRF axons in the IL of freely moving mice led to behavioral arrest and transient interruption of awake cortical activity. An afferent system with comparable morphological features was also found in the human IL. These data reveal an evolutionarily conserved ascending system that gates forebrain activity through fast and powerful synaptic inhibition of the IL.

Adaptive behavior depends on rapid initiation and termination of movements requiring fast communication and synchronized activity between the neocortex (for planning the movements[1–3]), the basal ganglia (for switching between behavioral regimes[4,5]) and the brainstem (for organization of motor commands[6–8]). Although our knowledge of brain circuits that organize motor sequences has greatly improved in the past decade, relatively little is known about the mechanisms that actively suspend ongoing behavior[9]. Furthermore, behavioral arrest and subsequent immobility are accompanied by the emergence of various types of slow cortical oscillations[10,11], suggesting that stop signals may also induce a standby state in forebrain circuits. The manner in which cessation of movements is linked to slow wave activity also remains unclear.

The intralaminar thalamic nuclei (IL) represent a potential key hub in this system because they receive the highest density of brainstem inputs in the thalamus[12] and have rich connectivity with frontal cortex and basal ganglia[13]. Injuries to the IL induce severely impaired movement initiation and can lead to a persistent vegetative state[14,15]. Conversely, deep brain stimulation of the IL in human patients with a minimally conscious state can reinstate voluntary movements[16]. However, direct evidence for the involvement of the IL in organizing behavior is still lacking as a result of our inability to transiently modify IL activity in a physiologically relevant manner.

Morphological analyses of mice expressing eGFP in glycinergic neurons have revealed an intense and nucleus-specific glycinergic innervation of the IL and midline thalamic nuclei[17] (**Supplementary Fig. 1**). Because most glycinergic projections arise in the brainstem[17], we investigated whether these projections might constitute an inhibitory pathway linking the brainstem and the thalamus and thereby controlling forebrain neuronal activity.

RESULTS

An inhibitory pathway from the PRF to the thalamus

Glycinergic fibers identified through expression of GlyT2 were found in both the IL and midline nuclear complexes[17] (**Supplementary Fig. 1**). More specifically, in the anterior IL, they were distributed in the centrolateral and paracentral nuclei and spread to the adjacent paralaminar part of the mediodorsal nucleus. We observed dense innervation also in the caudal IL (in the parafascicular nucleus) and scattered fibers in the nucleus posterior. In addition, the midline nuclei (paraventricular, intermediodorsal and centromedial nuclei) also received glycinergic inputs. We used retrograde neuronal tracing to localize the origin of the glycinergic fibers ($n = 6$) in the IL. The largest concentration of IL-projecting *Glyt2* (also known as *Slc6a5*)-*eGFP* cells was found in the ipsilateral oral and caudal pontine reticular nucleus (PnO and PnC, respectively; **Fig. 1a–d** and **Supplementary Figs. 2** and **3**). For brevity, we refer to the two nuclei collectively as PRF. In the ipsilateral PRF, 55.3% of the retrogradely labeled neurons were *Glyt2-eGFP* positive ($n = 765$ cell in 6 animals). Conversely, anterograde tracing from the PRF (injections centered

[1]Laboratory of Thalamus Research, Institute of Experimental Medicine, Hungarian Academy of Sciences, Budapest, Hungary. [2]Biology Institute of the Ecole Normale Supérieure, IBENS, Paris, France. [3]Inserm, U1024, Paris, France. [4]CNRS, UMR 8197, Paris, France. [5]Laboratory of Cerebral Cortex Research, Institute of Experimental Medicine, Hungarian Academy of Sciences, Budapest, Hungary. [6]Department of Pathology, St. Borbála Hospital, Tatabánya, Hungary. [7]Department of Psychiatry, St. Borbála Hospital, Tatabánya, Hungary. [8]Cold Spring Harbor Laboratory, Cold Spring Harbor, New York, USA. [9]Institute of Pharmacology and Toxicology, University of Zurich, Zurich, Switzerland. [10]Institute of Pharmaceutical Sciences, Swiss Federal Institute of Technology, Zurich, Switzerland. [11]These authors contributed equally to this work. Correspondence should be addressed to L.A. (acsady@koki.hu) or S.D. (dieudon@biologie.ens.fr).

Received 6 June 2014; accepted 20 January 2015; published online 23 February 2015; doi:10.1038/nn.3951

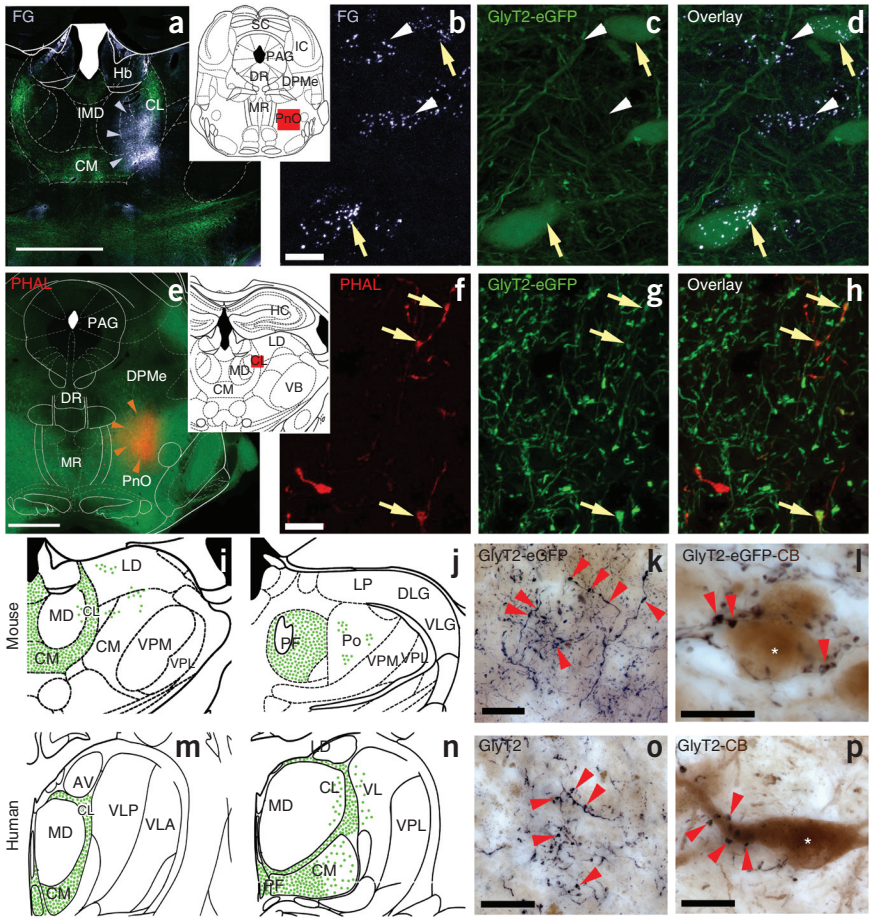

Figure 1 Glycinergic afferents in the mouse and human IL. (**a**) Injection site (arrowheads) of the retrograde tracer fluorogold (FG) into the IL of a *Glyt2-eGFP* mouse. (**b**–**d**) Retrogradely labeled GlyT2-eGFP–positive (arrows) and GlyT2-eGFP–negative (arrowheads) neurons in the PnO at the coronal level indicated in the inset. (**e**–**h**) Injection site (arrowheads) of the anterograde tracer PHAL into the PnO (**e**) and anterogradely labeled GlyT2-eGFP–positive fibers (arrows) in the IL (**f**–**h**) at the position shown in the inset. (**i**,**j**,**m**,**n**) Distribution of GlyT2 fibers in the mouse (**i**,**j**) and human (**m**,**n**) thalamus at two coronal levels. The figures represent cumulative data. (**k**,**l**,**o**,**p**) Light microscopic images of GlyT2-positive fibers and innervation of calbindin-positive cells via multiple contacts in the mouse (**k**,**l**) and human (**o**,**p**) IL. Asterisks indicate CB-positive cell bodies. Scale bars represent 1 mm (**a**,**e**) and 20 µm (**b**–**d**,**f**–**h**,**k**,**l**,**o**,**p**). CB, calbindin. For other abbreviations, see **Supplementary Figures 1** and **2**.

at the PnO; **Fig. 1e**–**h**) revealed that 65% of the ipsilateral pontothalamic terminals were *Glyt2-eGFP* immunoreactive in the IL ($n = 770$ boutons in 3 animals).

The ponto-thalamic pathway specifically innervates the IL also in the human brain[18,19]. To establish the existence of its inhibitory component in humans, we compared *Glyt2-eGFP* labeling in mice with post mortem human thalamic tissue samples ($n = 3$) immunostained for GlyT2. The distribution of GlyT2-immunopositive fibers was markedly similar in the thalamus of mice and man (**Fig. 1i**–**p**). Double immunostaining with calbindin (CB), which labels IL[20] revealed that multiple GlyT2-positive axon terminals innervated IL thalamocortical cells in both species (**Fig. 1l**,**p**).

At the electron microscopic level, *Glyt2-eGFP* terminals in the mouse IL ($n = 73$ terminals in 3 mice) established symmetrical synapses and puncta adhaerentia with the targeted thalamocortical neurons (**Fig. 2a**,**b**). 14 of the 16 terminals (87.5%) reconstructed in three dimensions established multiple (up to 14, mean = 6.7, s.d. = 3.6) closely spaced synapses (**Supplementary Fig. 4a**), always with a single postsynaptic partner. The *Glyt2-eGFP* terminals innervated significantly thicker dendrites (mean minor diameter = 0.9 ± 0.2 µm, $n = 68$) than randomly selected dendrites in the same neuropil (mean minor diameter = 0.5 µm, s.d. = 0.2 µm, $n = 228$; χ^2 test for homogeneity, $P = 2.2 \times 10^{-16}$, df = 2; **Fig. 2c**), indicating that they preferentially contacted proximal dendritic domains. The number of synaptic contacts correlated with postsynaptic dendrite diameter (linear regression, $n = 16$, R2 = 0.3354, $F = 7.066$, regression df = 1, residual df = 14, $P = 0.0187$; **Fig. 2d**) and showed a tendency to increase with bouton volumes ($n = 8$; **Supplementary Fig. 4b**). In one terminal, up to seven synapses could be found in a 1-µm radius of a given synapse ($n = 19$ synapses in 2 boutons, 83 intersynaptic distances; **Fig. 2e** and **Supplementary Fig. 4c**). This synaptic arrangement has been shown in other systems to promote rapid neurotransmitter pooling between active zones[21,22]. Electron microscopic analysis of the human tissue revealed that the morphological features of GlyT2 terminals in the IL matched their rodent counterparts (large size, multiple active zones, mitochondria and puncta adhaerentia, large caliber dendritic target; $n = 15$; **Fig. 2f**), although the posytsynaptic modifications appeared to be more complex. These morphological data indicate that a powerful, evolutionary conserved, inhibitory system targets IL neurons at strategic, proximal dendritic domains, potentially controlling synaptic integration and firing.

In the spinal cord, glycine immunoreactivity is frequently colocalized with GABA[23]. We therefore investigated the presence of GABA in *Glyt2-eGFP* terminals of the mouse IL. Postembedding GABA immunostaining revealed that 57 of 58 *Glyt2-eGFP*–positive terminals displayed GABA immunoreactivity (**Fig. 2b**). Furthermore, clusters of glycine receptors (GlyRs) and of the γ2 subunit of $GABA_A$Rs (GABAγ2Rs) were both juxtaposed to *Glyt2-eGFP* varicosities in the IL (**Fig. 2g** and **Supplementary Fig. 5**). The number of associated GABAγ2R and GlyR clusters per terminal (3.70 ± 2.45) displayed great variability (**Fig. 2h**). About 68% of the terminals were opposed to both GlyR and GABAγ2R clusters ($n = 2{,}014$, 4.57 ± 2.38 clusters), whereas 29% faced only GABAγ2R ($n = 848$, 1.89 ± 1.25) and 3% faced only GlyR clusters ($n = 81$, 1.12 ± 0.33 clusters per terminal). These data indicate that differential postsynaptic receptor accumulation may fine-tune synaptic transmission at the mixed inhibitory brainstem-IL synapses.

PRF-thalamic fibers evoke strong, non-depressing inhibition

To study the inhibitory impact of GlyT2 fibers on IL neurons we chose an optogenetic approach and injected the PRF of BAC transgenic *Glyt2-Cre* mice (**Supplementary Fig. 6a**–**c**) with adeno-associated viruses (AAVs) carrying a flex-ChR2-eYFP construct (ChR2-eYFP; **Supplementary Fig. 6d**–**i**). Following viral transgenesis, fibers expressing ChR2-eYFP were confined to the IL and midline nuclei (**Supplementary Fig. 6j**–**o**) and were immunoreactive for GlyT2,

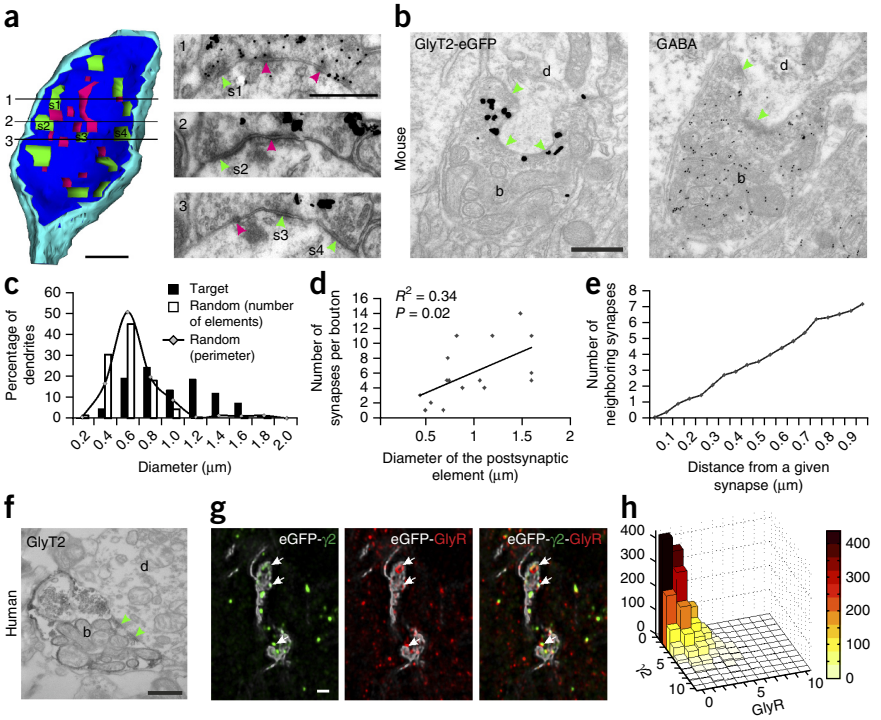

Figure 2 Glycinergic terminals in IL are multisynaptic, coexpress GABA and display variable postsynaptic receptor composition. (**a**) Three-dimensional reconstruction of a GlyT2-eGFP–positive terminal in IL from serial electron microscopic (EM) images, three of which are shown on the right. Green indicates synapses, magenta indicates puncta adherentia, dark blue indicates membrane of the terminal, light blue indicates glia, green arrowheads point to synapses and magenta arrowheads point to puncta adherentia. (**b**) Consecutive electron micrographs of a GlyT2-eGFP bouton (b) in the mouse IL immunostained for eGFP using preembedding silver staining (left), and for GABA using postembedding immunogold labeling (right). (**c**) Comparison of random dendritic diameters (white bars) in the IL and the diameter of targets postsynaptic to GlyT2-eGFP terminals (black bars). Random dendrite diameters are also shown and as the ratio of summated perimeter of the dendrites in each bin (black line with diamonds), which better reflect the available membrane surfaces. (**d**) Correlation between the synapse numbers of the GlyT2-eGFP boutons and the diameter of the postsynaptic IL dendrites. (**e**) The average number of synapses with increasing distances from a given synapse in eGFP boutons in the IL. (**f**) Electron micrograph of a GlyT2-immunopositive axon terminal in the human IL. Green arrowheads represent synapses. (**g**) White arrows point to colocalization of the γ2 subunit of $GABA_A$ receptors and of glycine receptors postsynaptic to *Glyt2-eGFP* terminals in mouse. (**h**) The cityscape plot represents the number of apposed GABAγ2R receptor and GlyR clusters per *Glyt2-eGFP* varicosity. d, dendrite in **b** and **f**. Scale bars represent 500 nm (**a**,**b**,**f**) and 1 µm (**g**).

confirming the specificity of our approach. We recorded thalamocortical cells of the IL in acute slices prepared from *Glyt2-Cre* mice after brainstem injection with the ChR2-eYFP construct (**Fig. 3a**,**b**). Broad field illumination with brief (1–2 ms) flashes of blue light reliably evoked outward synaptic currents, with average amplitudes of 68.45 ± 18.86 pA (n = 14 cells) at −40 mV (**Fig. 3c**). Light-evoked inhibitory postsynaptic currents (leIPSCs) followed illumination onset with short latency (3.09 ± 0.17 ms, n = 14 cells) and rapid rise and decay times (rise time: 0.54 ± 0.04 ms, n = 14; decay time: 6.18 ± 0.47 ms, n = 20). leIPSCs were blocked by tetrodotoxin (500 nM; 1.87 ± 0.65% of control, n = 7, Wilcoxon signed rank test, P = 0.018, W(7) = 0). Following co-application of the $GABA_A$R antagonist SR95531 (5 µM) and the GlyR antagonist strychnine (1 µM), the amplitude of the remaining leIPSCs was reduced to 2.80 ± 0.72% (n = 8 cells, Wilcoxon signed rank, P = 0.0011, W(8) = 0) of the control value, demonstrating the inhibitory nature of the optically activated synapses (**Fig. 3c**).

SR95531 alone decreased the amplitude of leIPSCs, on average, to 56.20 ± 7.55% (n = 22 cells). In individual IL neurons, this value varied between 0 and 100% (**Fig. 3d**,**e**), indicating that there was a large amount of variability in the ration of GABA/glycine receptor expression in IL neurons. Typical of mixed inhibitory synapses, SR95531 shortened the decay of the leIPSCs from 8.76 ± 0.83 ms to 6.18 ± 0.41 ms (n = 13, Wilcoxon signed rank test, P = 0.003, W(13) = 3), revealing significantly faster kinetics of the glycinergic component relative to the GABAergic component (**Fig. 3f**,**g**). This kinetic difference has been proposed to provide precise inhibitory control over the postsynaptic neurons[24].

Our anatomical analyses revealed that GlyT2 terminals establish several synapses. Multisynaptic inhibitory terminals are designed to evoke faithful responses even at high presynaptic firing rates[21,22]. Accordingly, we observed that trains of optical stimuli in the IL, delivered to ChR2-eYFP–expressing PRF fibers, at frequencies of 10–40 Hz reliably evoked leIPSCs trains without apparent decrease in amplitudes (**Fig. 3h** and **Supplementary Fig. 7a**), demonstrating the absence of prominent short-term depression. We further confirmed the dynamic behavior of the synapses by electrically evoking IPSCs (eIPSCs) in the IL following pharmacological isolation of the glycinergic component (**Supplementary Fig. 7b**,**c**). The eIPSCs were also non-depressing at all of the frequencies tested (range, 10–200 Hz). This indicates that the depression of leIPSCs found at 50 Hz (**Supplementary Fig. 7a**,**c**) was possibly a result of non-physiological effects of optogenetic activation[25] and confirms reliable inhibitory synaptic transmission at the PRF-IL synapse during high presynaptic firing rates.

We next tested the efficacy of sustained PRF-thalamic inhibition in controlling the discharge of thalamocortical IL neurons. leIPSPs evoked by 1-s stimulation trains at 20 Hz depressed the firing of IL cells to 32.27 ± 22.86% of the control pre-illumination period (n = 4 cells, paired t test, P = 0.025, t = 4.18; **Fig. 3i**). Taken together, these data demonstrate that PRF terminals can exert a fine-tuned, powerful inhibition in the thalamus, potentially controlling the activity of IL cells during behavior.

Inhibitory PRF-thalamic fibers evoke behavioral arrest

To study the behavioral effect of the PRF-IL inhibitory pathway, we optogenetically activated GlyT2 fibers in freely moving animals through unilateral optic fibers, chronically implanted in the IL. Light activation of GlyT2 terminals in the IL using 30-Hz stimulation trains at high laser intensities evoked a near-complete behavioral arrest for the duration of the stimulation (**Supplementary Movie 1**). All types of behavior were suspended (exploration, eating, grooming) 1–2 s following stimulation onset, whereas the posture of the animals

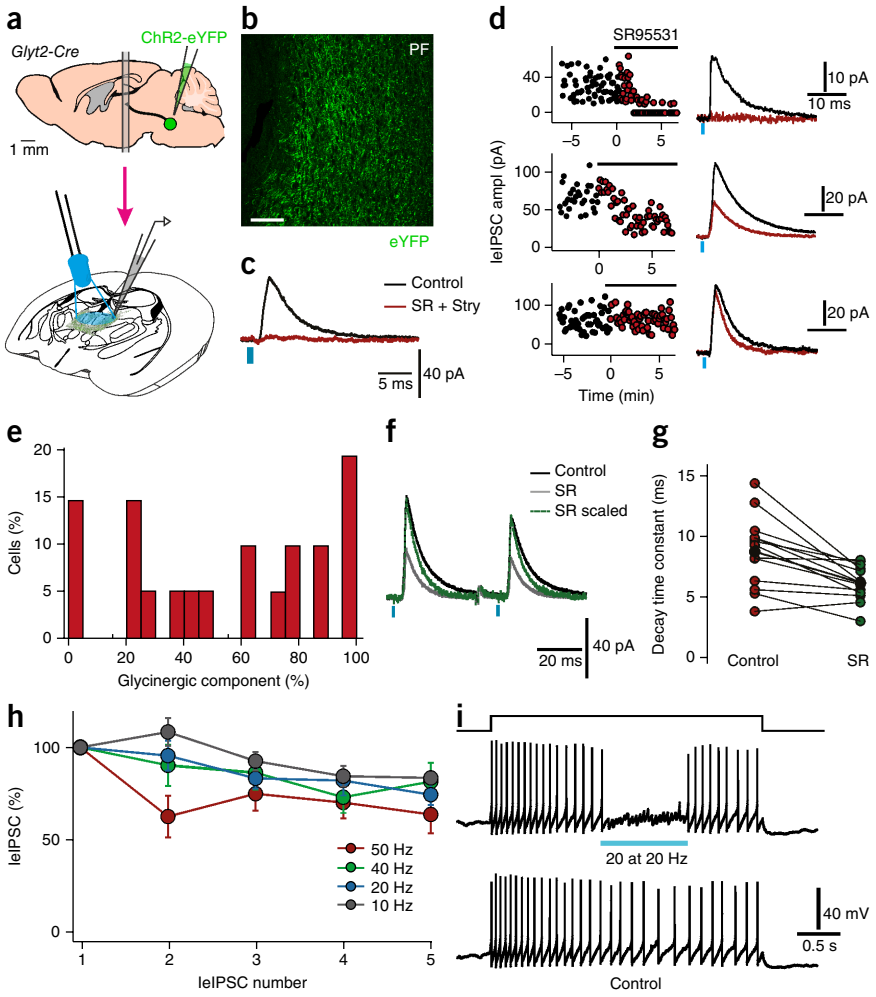

Figure 3 Glycinergic input evokes non-depressing inhibition and reduces IL cell firing. (**a**) Scheme of the experiment. (**b**) ChR2-eYFP–containing fibers in the IL. Scale bar represents 50 µm. (**c**) Averaged sample trace of IeIPSCs before (black trace) and after (red) application of gabazine and strychnine. (**d**) Variable mixed GABA/glycinergic phenotype of IeIPSCs. Three different examples are shown with only GABAergic (top), mixed GABA/glycinergic (center) and only glycinergic (bottom) transmission. (**e**) Ratio of IL cells showing various proportions of glycinergic IeIPSCs. (**f**,**g**) SR95531 application led to a substantial acceleration of the decay time course of the IeIPSCs. Shown are the averaged traces for a single recorded cell (**f**) and the pooled results for all the experiments (**g**). (**h**) Light-evoked responses displayed little depression during stimulation trains at different frequencies. Error bars represent ±s.e.m. (**i**) Activation of GlyT2 fibers interrupted firing of IL neurons recorded in the current-clamp configuration.

was maintained. The animals either became motionless, displaying only small head movements, or performed hypo/bradykinetic movements, which were frequently asymmetric with the animals turning contralateral to the stimulation side. After turning off the laser stimulation, spontaneous activity reappeared. Decreasing light intensity resulted in gradually increasing distance traveled during the stimulation periods (n = 3; **Supplementary Fig. 8**). Obvious signs of fear (piloerection, defecation) were absent and animals reintroduced to the same context did not display freezing behavior.

To quantify the behavioral change, we measured the distance traveled in the second half of 10-s stimulation periods (**Fig. 4**). Optogenetic activation of GlyT2 fibers decreased animal movements significantly with respect to the pre-illumination period to 30.88 ± 4.68% (n = 9 animals, ranging from 10.83 to 52.60%, Wilcoxon signed rank test, P = 0.008, W(9) = 0; **Fig. 4c**). The inhibition was absent in *Glyt2-Cre* mice injected with a double *loxP*-flanked AAV encoding just eYFP (111.05 ± 2.49% of the control, n = 5, Wilcoxon signed rank test, P = 0.89, W(5) = 7, with respect to the pre-illumination period; **Fig. 4c** and **Supplementary Movie 2**). The difference in traveled distance during laser illumination between test and control mice was highly significant (Mann-Whitney U test, P = 0.001, U(9.5) = 45).

Inhibitory PRF-thalamic fibers evoke slow oscillation

To identify the influence of the PRF-thalamic inhibitory projections on large scale forebrain loops, we recorded the local field potentials in freely moving mice (n = 7, local field potential, LFP) from motor cortical areas (**Fig. 5a**) that receive IL input[13] and project to PRF (**Supplementary Fig. 9**). Optogenetic activation of GlyT2 fibers in the

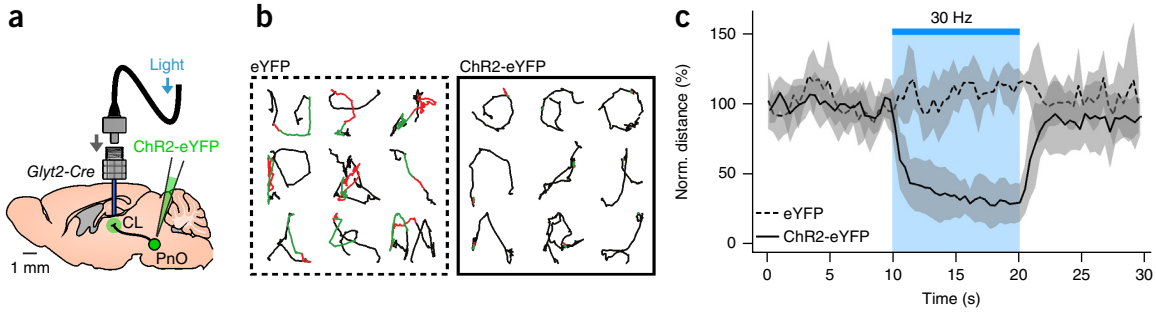

Figure 4 Activation of glycinergic afferents interrupts ongoing behavior. (**a**) Experimental design. (**b**) Mice trajectory during the first (red) and second (green) 5 s of optogenetic activation of GlyT2 fibers in the IL and during laser light shut off (black lines) in control (eYFP, left) and experimental (ChR2-eYFP, right) conditions. (**c**) Average movement of control (dashed trace) and optogenetically activated (continuous trace) mice before, during (blue bar) and after stimulation. Shading represents s.e.m.

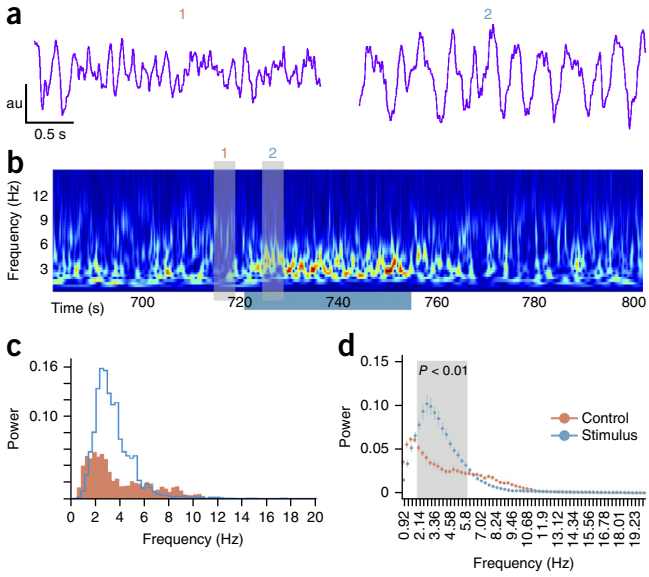

Figure 5 Activation of glycinergic afferents interrupts ongoing cortical activity. (**a**) Representative standardized frontal cortical LFP traces before (1) and during (2) the optogenetic activation of GlyT2 fibers in the IL. (**b**) Wavelet spectrum of the cortical LFP showing the 33-s-long activation period together with pre- and post-illumination period. Gray bars indicate the position of LFP samples in **a**. Warm colors indicate higher power. (**c**) Power spectra of the cortical LFPs in the 30 s preceding the stimulation (orange) and during photoactivation (blue) of the GlyT2 fibers in IL. (**d**) Statistical comparison of the power spectra of the stimulated and control periods in one representative animal ($n = 25$ stimulations). Gray bar indicates the frequency range which displayed statistically significant difference (2.14–5.8 Hz, Mann-Whitney U test). In this range, the highest P value was 0.00226 at 5.8 Hz (W = 457). All other P values were lower. Error bars represent the s.e.m. au arbitrary unit.

IL of awake animals for 33 s resulted in a marked modification of the ongoing cortical electrical activity. The low-amplitude high-frequency fluctuations, which dominate awake states, were abruptly replaced by large-amplitude slow oscillations ($n = 4$ animals, 47 stimulations; **Fig. 5a**,**b**). A significant increase (Mann-Whitney U test, $P < 0.01$) was evident in the frequency range of 2–6 Hz (**Fig. 5c**) compared with pre-illumination periods (**Fig. 5c**,**d**). Slow-wave activity disappeared following the termination of the stimulus (**Fig. 5b**).

Finally, we measured the neuronal activity of *Glyt2-eGFP*–positive neurons in the PRF during slow cortical oscillation *in vivo* using juxtacellular recording and labeling ($n = 11$ cells localized in PnO; **Fig. 6**, and **Supplementary Fig. 10**) under ketamine anesthesia, which is known to reproduce the main features of cortical slow wave oscillation[25]. 8 of 11 *Glyt2-eGFP* neurons fired high frequency clusters of action potentials (frequency, 2–23 Hz; within-cluster frequency, 12–100 Hz; mean = 41.34 ± 11.59) interspersed with silent periods. Two of these neurons were activated antidromically from the IL (**Supplementary Fig. 10b**). The activity of all *Glyt2-eGFP*–positive PnO units displaying clustered firing was correlated with the LFP and multiunit activity measured in the frontal cortex (**Fig. 6b** and **Supplementary Fig. 10d**,**f**,**h**). The phase preference of individual *Glyt2-eGFP* cells displayed a large heterogeneity and spanned the whole up and down cycle of the cortical slow oscillation (**Fig. 6f**). This indicates that, despite the fact that the majority of *Glyt2-eGFP*–positive cells activity is modulated by slow cortical oscillation in resting states, IL neurons may experience a continuous, tonic bombardment of phase-modulated firing from GlyT2 PnO cells. The data also show that the within-cluster firing frequency of PRF cells was in the range that was used for the *in vitro* short-term plasticity experiments and for the *in vivo* optogenetic activation that evoked behavioral arrest and slow cortical oscillations in the awake animals.

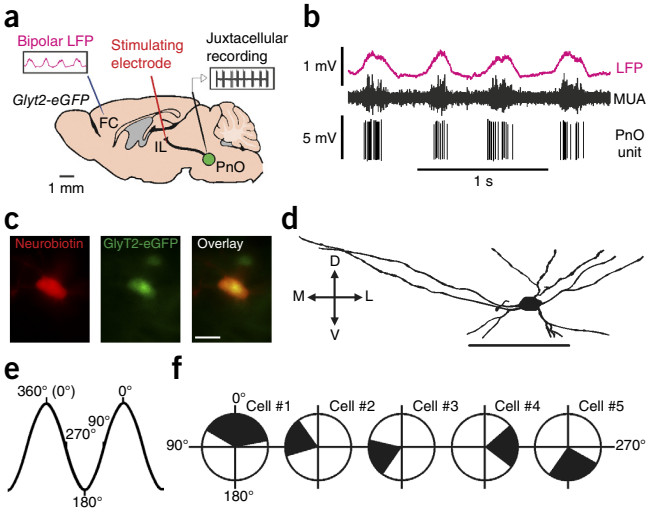

Figure 6 Activity of GlyT2-positive neurons in the PRF *in vivo* is linked to cortical slow oscillation. (**a**) Experimental design. (**b**) Spiking activity of a GlyT2 cell *in vivo* under ketamine-xylazine anesthesia (bottom trace) together with the cortical LFP (top trace) and filtered cortical multiunit activity (MUA, middle trace). (**c**) The recorded and neurobiotin filled cell display GlyT2-eGFP expression. (**d**) Neurolucida reconstruction of the recorded cell. (**e**,**f**) Phase distribution of the firing activity of five different GlyT2-eGFP–positive neurons relative to the cortical slow oscillation. One cycle is 360°, 0° peak of the UP state. Note the different phase preference of each cell. Scale bars represent 20 µm (**c**) and 100 µm (**d**).

DISCUSSION

Our experiments identified previously unknown IL-projecting GABA/glycinergic inhibitory neurons in the brainstem that exerted powerful control over the IL and cortical activity as well as on ongoing behavior. These neurons provided a link between brainstem and forebrain movement inhibition centers and promoted the establishment of the resting cortical state, which characterizes inactivity. Our data point to a conceptually novel form of brainstem-forebrain interaction wielding a substantial influence on major executive functions. This pathway appears to be conserved between mouse and human. We found marked similarities in the distribution of GlyT2 fibers in the thalamus, in the thalamic cell type and the dendritic domains innervated by the GlyT2 fibers, and in the ultrastructure of the terminals (**Figs. 1** and **2**). Recent diffusion tensor imaging data in humans clearly suggest the existence of a substantial ponto-thalamic pathway that terminates in the IL[18,19], suggesting that the GlyT2 inputs to IL arise from the same sources and are homologous in the two species. The mouse behavioral data, together with the evolutionary conserved nature of the system, are compatible with the role of the brainstem and IL in controlling human voluntary movements and consciousness[15,16,26].

PRF-thalamic inhibition with dual inhibitory phenotype

The vast majority of the PRF-thalamic terminals established multiple, closely spaced synapses and innervated large-caliber, proximal dendrites that allow faithful and reliable synaptic inhibition[21,27] in the IL.

Similar to many inhibitory neurons in the spinal cord[23], thalamic-projecting PRF cells displayed dual GABA/glycinergic phenotype. On the postsynaptic side, both the receptor composition at individual synapses and the synaptic responses of individual IL cells to afferent activation displayed a heterogeneous GABA/glycinergic ratio (**Fig. 3**). Although the neurotransmitter content of presynaptic axons can influence postsynaptic receptor activation[28], preferential expression of $GABA_A$Rs or GlyRs by the postsynaptic cell seems to be the main determinant of the IPSC phenotype in mixed systems[29,30]. Our anatomical and physiological results also support a postsynaptic choice for neurotransmitter receptor clustering. Given that GABAergic and glycinergic IPSCs have different decay time constant, this variability translates to inhibitory responses with variable kinetics. This allows individual postsynaptic neurons to shape their inhibitory control exerted by mixed GABA/glycinergic input. Kinetic differences between glycinergic and GABAergic components of PRF-thalamic IPSCs may also help to tune the inhibition window through nonlinear interactions of the GABAergic and glycinergic components[24]. Overall, the PRF-thalamic inhibitory system is ideally suited to perform fine control of the thalamo-cortical circuits, but the exact functional consequences of heterogenous inhibitory kinetics to the output of IL at the systems level remains to be determined.

Inhibitory PRF effects on movements and cortical activity

Behavioral arrest and the emergence of slow-wave activity were induced by activation of inhibitory PRF fibers in IL (**Figs. 4** and **5**). The exact mechanisms underlying these two effects remain to be established. However, our data are compatible with previous results indicating that PRF is an important center of movement inhibition and that PRF may be the origin of an ascending arrest signal[31–33].

The thalamic targets of the ascending inhibitory PRF fibers, the IL, have the necessary connectivity required for the generation of both behavioral arrest and slow oscillations. One of the main targets of IL nuclei is the striatum[13,34]. It has been known that activation of the indirect striatal pathway leads to movement inhibition[35], similar to the arrest induced in our experiments by PRF fiber stimulation in the IL (**Fig. 4**). On the other hand, activation of the direct pathway produces exacerbated motor activity[35]. If both pathways are activated in a balanced manner, movements will again be facilitated[36]. Given that IL innervate both the direct and the indirect striatal pathways[37] and exert strong excitation on their targets, they may contribute to this balanced drive observed during movement. As a consequence, their inhibition by PRF fibers can produce motor disturbances. The second effect, the emergence of slow-wave activity in the cortex, can be linked to the intrinsic properties and the cortical projection of IL thalamocortical neurons[13]. In general, inhibition of thalamic cells can lead to spontaneous, slow, rhythmic oscillations[38], which could resonate with the frontal cortical targets of the IL, the most prominent region for slow cortical activity. It should be noted that the optogenetic activation of PRF axons in the thalamus can also induce antidromic spikes that may propagate to putative non-thalamic targets of PRF cells. These effects remain to be investigated.

We propose that the two consequences of PRF fiber activation in IL are functionally linked. Immobility or stand-by states are characterized by various types of slow oscillations[10,39]. During these inactive states, 'offline' analysis of previously learned events occurs via replay of the previous neuronal activity, which is temporally coordinated by the slow oscillations[40]. It has also been suggested that slow oscillations are necessary to perform essential neuronal maintenance functions[41]. In any scenario, linking behavioral arrest and slow oscillations through a single control system, the ascending pontothalamic pathway, would be beneficial for controlling behavioral and brain states. Finally, it should be noted that our data do not rule out that the ascending system that we describe participates in other brain functions, such as arousal, sleep regulation or pain perception.

METHODS

Methods and any associated references are available in the online version of the paper.

Note: Any Supplementary Information and Source Data files are available in the online version of the paper.

ACKNOWLEDGMENTS

The excellent technical help of K. Faddi, L. Barna and G. Goda is gratefully acknowledged. The authors wish to thank the Nikon Microscopy Center at the Institute of Experimental Medicine, Nikon Austria GmbH and Auro-Science Consulting for kindly providing microscopy support. This work was supported by the Hungarian Scientific Research Fund (OTKA T109754 and T75676), the National Office for Research and Technology (NKTH-ANR-09-BLAN-0401, Neurogen), the Hungarian Korean Joint Laboratory Program, the Hungarian Brain Research Program (grant no. KTIA_13_NAP-A-I/1) and the Wellcome Trust (fWT094513) to L.A., and an Advanced Investigator ERC (DHISP 250128) to H.U.Z. We also received support from the CNRS, INSERM, the Ecole Normale Supérieure, and under the program 'Investissements d'Avenir' launched by the French Government and implemented by the ANR, with the references: ANR-10-LABX-54 MEMO LIFE and ANR-11-IDEX-0001-02 PSL* Research University. B.H. received support from the Swartz Foundation and Marie Curie International Outgoing Fellowship in the EU Seventh Framework Programme for Research and Technological Development.

AUTHOR CONTRIBUTIONS

K.G. and V.P. performed the tract tracing and its quantitative analysis. K.G. organized the anatomical experiments and carried out the electron microscopic analysis, three-dimensional electron microscopy reconstructions and quantification. M.A.D. performed the *in vitro* physiological experiments. M.A.D., V.P. and G.P.D. performed the optogenetics in freely moving animals. C.V.R. carried out the quantitative receptor localization. Z.M. and L.H. performed the preparation of human material. V.P. and H.B. carried out the juxtacellular recordings. B.H. performed the analysis of juxtacellular recordings. H.W. and H.U.Z. accomplished the generation and characterization of transgenic animals. M.A.D. and S.D. organized the *in vitro* and freely moving optogenetic experiments. L.A. organized the anatomical and *in vivo* physiological experiments and coordinated the project. K.G., M.A.D., S.D. and L.A. wrote the manuscript.

COMPETING FINANCIAL INTERESTS

The authors declare no competing financial interests.

1. Drew, T., Andujar, J.-E., Lajoie, K. & Yakovenko, S. Cortical mechanisms involved in visuomotor coordination during precision walking. *Brain Res. Rev.* **57**, 199–211 (2008).
2. Lemon, R.N. Descending pathways in motor control. *Annu. Rev. Neurosci.* **31**, 195–218 (2008).
3. Rizzolatti, G. & Luppino, G. The cortical motor system. *Neuron* **31**, 889–901 (2001).
4. Graybiel, A.M. Habits, rituals, and the evaluative brain. *Annu. Rev. Neurosci.* **31**, 359–387 (2008).
5. Isoda, M. & Hikosaka, O. Cortico-basal ganglia mechanisms for overcoming innate, habitual and motivational behaviors. *Eur. J. Neurosci.* **33**, 2058–2069 (2011).
6. Marder, E. & Calabrese, R.L. Principles of rhythmic motor pattern generation. *Physiol. Rev.* **76**, 687–717 (1996).
7. Rossignol, S., Dubuc, R. & Gossard, J.-P. Dynamic sensorimotor interactions in locomotion. *Physiol. Rev.* **86**, 89–154 (2006).
8. Hajnik, T., Lai, Y.Y. & Siegel, J.M. Atonia-related regions in the rodent pons and medulla. *J. Neurophysiol.* **84**, 1942–1948 (2000).
9. Klemm, W.R. Behavioral arrest: in search of the neural control system. *Prog. Neurobiol.* **65**, 453–471 (2001).
10. Buzsaki, G. *Rhythms of the Brain* (Oxford University Press, 2006).
11. Cabral, J., Kringelbach, M.L. & Deco, G. Exploring the network dynamics underlying brain activity during rest. *Prog. Neurobiol.* **114**, 102–131 (2014).
12. Krout, K.E., Belzer, R.E. & Loewy, A.D. Brainstem projections to midline and intralaminar thalamic nuclei of the rat. *J. Comp. Neurol.* **448**, 53–101 (2002).

13. Groenewegen, H.J. & Berendse, H.W. The specificity of the "nonspecific" midline and intralaminar thalamic nuclei. *Trends Neurosci.* **17**, 52–57 (1994).
14. Bogen, J.E. On the neurophysiology of consciousness. I. An overview. *Conscious. Cogn.* **4**, 52–62 (1995).
15. Kinney, H.C., Korein, J., Panigrahy, A., Dikkes, P. & Goode, R. Neuropathological findings in the brain of Karen Ann Quinlan: the role of the thalamus in the persistent vegetative state. *N. Engl. J. Med.* **330**, 1469–1475 (1994).
16. Schiff, N.D., Giacino, J., Kalmar, K. & Victor, J. Behavioural improvements with thalamic stimulation after severe traumatic brain injury. *Nature* **448**, 600–603 (2007).
17. Zeilhofer, H.U. *et al.* Glycinergic neurons expressing enhanced green fluorescent protein in bacterial artificial chromosome transgenic mice. *J. Comp. Neurol.* **482**, 123–141 (2005).
18. Yeo, S.S., Chang, P.H. & Jang, S.H. The ascending reticular activating system from pontine reticular formation to the thalamus in the human brain. *Front. Hum. Neurosci.* **7**, 416 (2013).
19. Edlow, B.L. *et al.* Neuroanatomic connectivity of the human ascending arousal system critical to consciousness and its disorders. *J. Neuropathol. Exp. Neurol.* **71**, 531–546 (2012).
20. Jones, E.G. *The Thalamus* (Cambridge University Press, 2007).
21. Wanaverbecq, N. *et al.* Contrasting the functional properties of GABAergic axon terminals with single and multiple synapses in the thalamus. *J. Neurosci.* **28**, 11848–11861 (2008).
22. Telgkamp, P., Padgett, D.E., Ledoux, V.A., Woolley, C.S. & Raman, I.M. Maintenance of high-frequency transmission at Purkinje to cerebellar nuclear synapses by spillover from boutons with multiple release sites. *Neuron* **41**, 113–126 (2004).
23. Todd, A.J. GABA and glycine in synaptic glomeruli of the rat spinal dorsal horn. *Eur. J. Neurosci.* **8**, 2492–2498 (1996).
24. Russier, M., Kopysova, I.L., Ankri, N., Ferrand, N. & Debanne, D. GABA and glycine co-release optimizes functional inhibition in rat brainstem motoneurons *in vitro*. *J. Physiol.* (*Lond.*) **541**, 123–137 (2002).
25. Chauvette, S., Crochet, S., Volgushev, M. & Timofeev, I. Properties of slow oscillation during slow-wave sleep and anesthesia in cats. *J. Neurosci.* **31**, 14998–15008 (2011).
26. Parvizi, J. & Damasio, A.R. Neuroanatomical correlates of brainstem coma. *Brain* **126**, 1524–1536 (2003).
27. Bokor, H. *et al.* Selective GABAergic control of higher-order thalamic relays. *Neuron* **45**, 929–940 (2005).
28. Lu, J. *et al.* Postsynaptic positioning of endocytic zones and AMPA receptor cycling by physical coupling of dynamin-3 to Homer. *Neuron* **55**, 874–889 (2007).
29. Dugué, G.P., Dumoulin, A., Triller, A. & Dieudonné, S. Target-dependent use of co-released inhibitory transmitters at central synapses. *J. Neurosci.* **25**, 6490–6498 (2005).
30. Rousseau, C.V. *et al.* Mixed inhibitory synaptic balance correlates with glutamatergic synaptic phenotype in cerebellar unipolar brush cells. *J. Neurosci.* **32**, 4632–4644 (2012).
31. Elazar, Z. & Paz, M. Catalepsy induced by carbachol microinjected into the pontine reticular formation of rats. *Neurosci. Lett.* **115**, 226–230 (1990).
32. Brudzyński, S.M. & Mogenson, G.J. The role of the nucleus reticularis tegmenti pontis in locomotion: a lesion study in the rat. *Brain Res. Bull.* **12**, 513–520 (1984).
33. Cheng, J.T., Schallert, T., De Ryck, M. & Teitelbaum, P. Galloping induced by pontine tegmentum damage in rats: a form of "Parkinsonian festination" not blocked by haloperidol. *Proc. Natl. Acad. Sci. USA* **78**, 3279–3283 (1981).
34. Smith, Y. *et al.* The thalamostriatal system in normal and diseased states. *Front. Syst. Neurosci.* **8**, 5 (2014).
35. Kravitz, A.V. *et al.* Regulation of parkinsonian motor behaviours by optogenetic control of basal ganglia circuitry. *Nature* **466**, 622–626 (2010).
36. Tecuapetla, F., Matias, S., Dugue, G.P., Mainen, Z.F. & Costa, R.M. Balanced activity in basal ganglia projection pathways is critical for contraversive movements. *Nat. Commun.* **5**, 4315 (2014).
37. Doig, N.M., Moss, J. & Bolam, J.P. Cortical and thalamic innervation of direct and indirect pathway medium-sized spiny neurons in mouse striatum. *J. Neurosci.* **30**, 14610–14618 (2010).
38. Leresche, N., Lightowler, S., Soltesz, I., Jassik-Gerschenfeld, D. & Crunelli, V. Low-frequency oscillatory activities intrinsic to rat and cat thalamocortical cells. *J. Physiol.* (*Lond.*) **441**, 155–174 (1991).
39. Poulet, J.F.A. & Petersen, C.C.H. Internal brain state regulates membrane potential synchrony in barrel cortex of behaving mice. *Nature* **454**, 881–885 (2008).
40. Ji, D. & Wilson, M.A. Coordinated memory replay in the visual cortex and hippocampus during sleep. *Nat. Neurosci.* **10**, 100–107 (2007).
41. Vyazovskiy, V.V. & Harris, K.D. Sleep and the single neuron: the role of global slow oscillations in individual cell rest. *Nat. Rev. Neurosci.* **14**, 443–451 (2013).

ONLINE METHODS

Anatomy. For the tract tracing, receptor localization and electron microscopic experiments, a total of 25 adult (older than 45 d) male *Glyt2-eGFP* mice were used. Mice were entrained to a 12-h light/dark cycle with food and water available *ad libitum*. Experimental procedures were approved by the Institute of Experimental Medicine Protection of Research Subjects Committee, the Food Safety and Animal Health Office of the Pest District Government Bureau (Budapest, Hungary), the Veterinäramt des Kantons Zürich (Switzerland) or the Centre National de la Recherche Scientifique (France).

Surgery. Surgery and experiments were done under ketamine/xylazine anesthesia (ketamine, 83 mg per kg of body weight; xylazine, 3.3 mg per kg).

Retrograde tracing. To identify brainstem neurons projecting to the thalamus, Fluorogold (FG) was injected iontophoretically (0.6 µA, 2-s on/off period, 10-min duration) into the intralaminar thalamus of *Glyt2-eGFP* mice under ketamine/xylazine anesthesia ($n = 6$ unilaterally and $n = 2$ bilaterally; capillary tip diameter = 20 µm), according to the following coordinates: AP, Br −1.5 mm to −1.8 mm; Lat, 0.7 mm, DV, −3.2 mm. After 3 d, the mice were perfused through the heart using fixative solution containing 0.1% glutaraldehyde (wt/vol) and 4% paraformaldehyde (wt/vol). The thalamus and the brainstem were cut coronally (50–60-µm slices), cryoprotected and frozen above liquid nitrogen. To identify cortical inputs to PnO, in a separate set of experiments ($n = 4$) FG was injected into the PnO (2 µA, 7-s on/off period, 15-min duration) at the following coordinates: AP, −4.4 mm; ML, −0.8 to −1 mm; DV, 4.2 mm. After 5–7 d of survival the animals were perfused and the entire brain was sectioned in the coronal plain.

Anterograde tracing. To visualize pontothalamic fibers, *Phaseolus vulgaris* leucoagglutine (PHAL, $n = 3$ unilateral) was iontophoretically injected (4 mA, 7-s on/off period, 10-min duration) into the oral or caudal pontine nucleus (PnO-PnC) of *Glyt2-eGFP* mice (50-µm capillary tip diameter) using the following coordinates: AP, Br −4.3 mm to −4.4 mm; Lat, 0.8 mm; V, −4.0 mm. After 1 week, the animals were perfused and the brains were sectioned as described above.

Immunocytochemistry. Fluorogold was visualized with a rabbit anti-Fluorogold antibody (1:10,000 to 1:20,000, Chemicon, AB 153) followed by either 1-nm gold particle–conjugated goat anti-rabbit (1:50, Amersham, RPN-470) and silver intensification (Aurion R-Gent SEM LM-silver enhancement kit, 20–22 min), or Alexa 594–conjugated goat anti-rabbit antibody (1:500, Molecular Probes A-11012). For identifying the cortico-PnO projection, the primary antiserum (1:30,000) was followed by biotinylated goat anti-rabbit (1:300, Vector, BA 1000) and avidin biotin horseradish peroxidase complex (ABC, 1:300, Vector, PK-6100). Nickel-intensified di-amino-benzidine (Ni-DAB, black reaction product) was then used as a chromogen. PHAL was visualized by rabbit anti-PHAL (1:10,000, Vector, AS-2300), and Alexa 594–conjugated goat anti-rabbit for fluorescent microscopy.

To visualize *Glyt2-eGFP* fibers with light microscopy the sections were treated with mouse anti-eGFP antibody (1:20,000, Molecular Probes, A11120) followed by biotinylated horse anti-mouse (1:300, Vector, BA 2000), avidin biotin horseradish peroxidase complex (ABC, 1:300, Vector) and Ni-DAB. To label the postsynaptic targets of *Glyt2-eGFP* fibers in the IL, the eGFP-Ni-DAB immunoreaction was followed by a treatment with rabbit anti-calbindin (1:20,000, Swant, CB 38) and rabbit ImmPRESS (1:2, Vector, MP-7401). The calbindin immunostaining was visualized by DAB alone yielding a brown reaction product.

To verify the specificity of the *Glyt2-eGFP* mouse line, coronal sections of the thalamus from *Glyt2-eGFP* mice were treated with guinea pig anti-GlyT2 antibody (1:10,000, Chemicon, AB 1773) followed by Cy3-conjugated donkey anti-guinea pig (1:500, Jackson, 706-166-148). All GlyT2-positive terminals examined ($n = 106$) displayed eGFP signal, whereas 95% of the eGFP terminals ($n = 311$) were immunopositive for GlyT2 ($n = 2$ animals).

The results of these light microscopic experiments were obtained either with a Zeiss Axioplan 2 fluorescent microscope and a digital camera (Olympus DP70), with a Zeiss Axio Imager M1 microscope coupled to an AxioCam HrC digital camera, or with a Nikon AR1 confocal microscope.

GABA and glycine receptor localization. Methods for immunohistochemical staining followed the protocols described in detail earlier[30].

Tissue fixation. Adult *Glyt2-eGFP* mice were deeply anesthetized with intraperitoneal injections of sodium pentobarbital (60 mg per kg body weight) and perfused through the ascending aorta with phosphate-buffered saline (PBS), followed by 50 ml of 4% freshly depolymerized paraformaldehyde (wt/vol) in 0.1 M PBS, pH 7.4, at 4 °C. Brains were then dissected and postfixed in 4% paraformaldehyde overnight at 4 °C, before embedding in paraffin.

Tissue preparation and labeling. Sections were cut at a thickness of 7 µm. After removing paraffin, sections were processed in a decloaking chamber (Biocare Medical) using a citrate buffer–based antigen retrieval medium (Biocare Medical) for 20 min at 110–115 °C. They were then processed in PBS with 15% methanol (vol/vol) and 0.3% H_2O_2 (vol/vol) to block endogenous peroxidase activity. Aldehyde groups were removed by incubating the sections in sodium borohydride (1%, wt/vol) in PBS. After these treatments, the slices were incubated in a blocking PBS-based solution containing cold-water fish-skin gelatin (0.1%, vol/vol) and 0.1% Triton X-100 (vol/vol). Tissues were then incubated overnight at 4 °C with the following primary antibodies: chicken anti-GFP (1:1,000, Aves labs, GFP 1020), rabbit anti-GABAa receptor gamma 2 subunit (1:1,500, Synaptic Systems, 224 003), mouse anti-GlyR (1:1,000, Synaptic Systems, 146 011), guinea pig anti-VIAAT (1:1,500, Synaptic Systems, 113 004 data not shown). Primary antibodies were revealed by incubation for 2 h with secondary antibodies coupled to either Alexa Fluor-488 (Invitrogen, A-11039) or DyLight 488, (Jackson ImmunoResearch, 703-485-155) DyLight 549, Jackson ImmunoResearch, 711-505-152 and 715-505-150) and DyLight 649 (Jackson ImmunoResearch, 715-495-150 and 711-495-152). Sections were finally mounted using Prolong Gold Antifade Reagent (Invitrogen). For all experiments, control sections were incubated without primary antibodies.

Image acquisition and analysis. Image stacks were acquired using a confocal microscope (SP2, Leica Microsystems or Nikon A1R) with a 63× oil-immersion objective. For image deconvolution, point-spread functions (PSFs) for multiple wavelengths were measured with subresolution (175 nm) beads (PS-Speck; Invitrogen), embedded in 7.5% gelatin and mounted in Prolong Gold. Bead images were then extracted from image stacks using a custom routine in ImageJ (W. Rasband, US National Institutes of Health), and averaged. Image stacks of the regions of interest were deconvolved using the Iterative Deconvolve 3D ImageJ plugin (R. Dougherty, http://www.optinav.com/imagej.html), and particles were subsequently analyzed using a custom version of the threshold-based Object Counter 3D ImageJ plugin (F. Cordelières & J. Jackson, http://rsbweb.nih.gov/ij/plugins/track/objects.html). To isolate terminals, images were thresholded, and axons were removed by erosion. Terminals were then dilated to their original size and used as masks on the thresholded image to preserve their precise morphologies. Detected particles where defined as regions of interests (ROIs) using the ImageJ 3D ROI manager[42]. The global density was measured as the number of particles divided by the volume of the three-dimensional image stack. To measure distances between receptors and terminal surfaces, terminals were converted to three-dimensional binary masks. The masks were then gradually dilated and the number of particles falling under a mask counted for each step. This count was then normalized by the volume of the added shell. The resulting distance density plot were fitted with the sum of a Gaussian function centered close to zero, representing the clusters associated to the varicosity (putatively on the postsynaptic element), and of a sigmoidal function of the form $Y = 1/(1 + \exp(-(X - A)/X_0))$, representing randomly distributed clusters in the surrounding tissue. The receptor clusters specifically associated with a terminal were taken as those falling within a distance of 600 nm from the terminal. Each ROI was isolated and the given terminal inflated to the specified distance. Receptors falling in this volume were then counted.

Results were processed using custom routines written in GNU R (R Development Core Team, 2013; http://www.r-project.org/) and Matlab (MathWorks). Since no difference in the measured variables could be observed between distinct intralaminar nuclei, data were pooled for statistics.

Electron microscopy. To explore the ultrastructure of the axon terminals with electron microscopy, mice were perfused with a sequential low pH/high pH fixative including 0.5% glutaraldehyde. eGFP was visualized using the silver-intensified preembedding gold method (mouse anti eGFP 1:1,000 followed by 1-nm gold particle-conjugated goat anti-mouse; for details, see ref. 21). All sections

were treated with OsO_4 (0.5%, vol/vol, for 20 min in 4 °C in 0.1 M PBS), dehydrated in ethanol and acetonitrile, and embedded in Durcupan (ACM, Fluka). Tissue blocks from IL ($n = 3$) containing silver-intensified gold-labeled terminals were re-embedded and series of 200–300 ultrathin sections (60 nm thick) were cut with an Ultramicrotome. Alternate sections were mounted on copper and nickel grids. Postembedding GABA immunostaining was carried out on nickel grids as described previously[43]. Serial electron micrographs were taken with a Megaview digital camera running on a HITACHI 7100 electron microscope. For two-dimensional measurements, ITEM software (Olympus Soft Imaging System) was used. The minor diameters of dendrites targeted by eGFP-positive terminals and of randomly selected dendrites were measured in three non-consecutive sections, and compared using the Chi-square homogeneity test. To establish the possible correlation between the bouton volume and the number of synapses, the latter were counted in all the sections containing the bouton. A linear regression was then calculated.

Reconstruct software was applied to reconstruct the terminals in three dimensions. The sections were aligned with the 'linear alignment' function that can partially compensate for individual section distortions caused by sectioning. Membranes, synapses and the covering surface of associated glia elements were reconstructed in terminals with preserved ultrastructure. Terminal volume, largest three-dimensional diameter and pair-wise synapse distances along the active surface were calculated. For further details on reconstructions, see ref. 21.

Processing of human tissue. Control human thalamic tissues ($n = 3$) were obtained from a male (74 years old) and two female (59 and 76 years old) subjects who died from causes not linked to brain diseases. None of them had a history of neurological disorders. The three subjects were processed for autopsy in Saint Borbála Hospital, Tatabánya, Department of Pathology. Informed consent was obtained for the use of brain tissue and for access to medical records for research purposes. Tissue was obtained and used in a manner compliant with the Declaration of Helsinki. All procedures were approved by the Regional and Institutional Committee of Science and Research Ethics of Scientific Council of Health (ETT TUKEB 31443/2011/EKU (518/PI/11)).

Brains were removed 4–5 h after death. The internal carotid and the vertebral arteries were cannulated, and the brains were perfused first with physiological saline (1.5 l in 30 min) containing heparin (5 ml), followed by a fixative solution containing 4% paraformaldehyde, 0.05% glutaraldehyde and 0.2% picric acid (vol/vol) in 0.1 M PB, pH = 7.4 (4–5 l in 1.5–2 h). The thalamus was removed from the brains after perfusion, and was postfixed overnight in the same fixative solution, except for glutaraldehyde, which was excluded. Subsequently, 50-µm-thick coronal sections were obtained for immunohistochemistry using a Leica VTS-1000 Vibratome (Leica Microsystems). The sections were incubated with a guinea pig anti-GlyT2 antibody (1:10,000, Chemicon, AB 1773), and the signal was visualized with the DAB-Ni reaction described above. The sections were then treated with OsO_4 (1.0% for 40 min. in 4 °C in 0.1 M PBS), dehydrated in ethanol and acetonitrile, and embedded in Durcupan (ACM, Fluka). Ultrathin sections were cut with an Ultramicrotome from blocks containing GlyT2-positive fibers. In some cases, postsynaptic IL neurons were visualized using mouse anti-calbindin antiserum and DAB reaction. In these cases, glucose (7%, wt/vol) was added to the OsO_4 solution to preserve the color difference.

Generation of *Glyt2-Cre* BAC transgenic mice. *Glyt2-Cre* BAC transgenic mice have been generated essentially as described previously for the *Glyt2-eGFP* BAC transgenic mice[17]. In brief, homologous recombination in bacteria was used to introduce the Cre coding sequence into the BAC-DNA (clone RP23-365E4). Pronuclei of fertilized C57BL/6 oocytes were injected with the modified BAC DNA. The resulting *Glyt2-Cre* mouse lines were maintained on a C57BL/6J background. Cre expression pattern was compared to the expression of eGFP in the well-characterized *Glyt2-eGFP* mouse line. In the CNS of *Glyt2-Cre* / *Glyt2-eGFP* double transgenic mice Cre expression was highly overlapping with eGFP expression (Foster, E., H.W., Broll, I., Haueter, S., Tudeau, L., Jegen, M., Bösl, M.R. & H.U.Z., unpublished observations). Genotyping was performed with the following primers; GlyT2Cre-fwd 5-GGGTGACCAAGGTAGGCTGAATG-3 and GlyT2Cre-rev 5-CCTGGCGATCCCTGAACATG-3.

The selectivity of CRE expression was also demonstrated by crossing the *Glyt2-Cre* and the *Glyt2-eGFP* mice lines and performing immunostaining for the Cre-protein (mouse anti-CRE, 1:10,000. Millipore, followed by Cy3-conjugated donkey anti-mouse, 1:500, 715-165-151). We found that, of 198 Cre-positive neurons, 196 (99%) were also eGFP positive (**Supplementary Fig. 6**).

Stereotactic injections. All optogenetic experiments were performed on adult (>3 months old) *Glyt2-Cre* mice. Mice were anesthetized with an intraperitoneal injection of ketamine-xylazine (200 and 10 mg per kg) and placed inside a stereotactic apparatus (Kopf Instruments). An AAV2/1.EF1α.DIO.hChR2(H134R).eYFP virus, based on Addgene plasmid 20298 and produced at the Laboratory of Gene Therapy (INSERM UMR 1089), was injected in the right side of the PnO, at the following coordinates: Bregma ML, +0.7 mm ; AP, 4.3 mm; DV, −4.8 mm. For the *in vivo* control experiments described in **Figure 4**, PnO neurons were transfected using an AAV2/1.EF1α.DIO.eYFP virus, based on Addgene plasmid 27056 and produced by the Vector Core facility of the University of Pennsylvania.

Injections were performed using pipettes pulled from graduated capillaries, at a rate of 100–150 nl min^{-1} for a total volume of 1.5–2 µl. *In vitro* and *in vivo* optogenetic stimulation experiments were all performed at least 4 weeks after viral injection.

Slice preparation. *In vitro* electrophysiological experiments were performed on coronal slices from the thalamus of virus injected *Glyt2-Cre* mice. Slices were prepared as described previously[29]. Briefly, mice were anesthetized with isofluorane before decapitation. After isolation, the portion of the brain containing the thalamus was placed in bicarbonate-buffered saline (BBS) at 2–5 °C for a few minutes. Slices (300 µm) were then cut using an HM650V vibratome (Microm). The slicing procedure was performed in an ice-cold solution containing (in mM): 130 potassium gluconate, 15 KCl, 0.05 EGTA, 20 Hepes, 25 glucose, 1 $CaCl_2$ and 6 $MgCl_2$, supplemented with 0.05 D-APV, and tetrodotoxin at 200 nM. Slices were then transferred for a few minutes to a solution containing (in mM): 225 D-mannitol, 2.5 KCl, 1.25 NaH_2PO_4, 25 $NaHCO_3$, 25 glucose, 1 $CaCl_2$ and 6 $MgCl_2$, and finally stored for the rest of the experimental day at 33 °C in oxygenated BBS, containing: 115 NaCl, 2.5 KCl, 1.6 $CaCl_2$, 1.5 $MgCl_2$, 1.25 NaH_2PO_4, 26 $NaHCO_3$ and 30 glucose (pH 7.4 after equilibration with 95% O_2 and 5% CO_2). For all recordings, slices were continuously superfused with oxygenated BBS at 32–34 °C.

Electrophysiology and *in vitro* optogenetic stimulation. *In vitro* electrophysiological recordings were preferentially performed from cells of the central lateral and the parafascicular nuclei. The nuclei were clearly recognizable by the distribution of ChR2-eYFP–positive fibers following virus injection in the pons. Cells were identified and patched in the transmitted deep red light with which slices were visualized using a CoolSnap HQ CCD camera (Photometrics) run by Metamorph software (Universal Imaging) and mounted on a Slicescope microscope (Scientifica). Recording pipettes were pulled from borosilicate glass capillaries and had a resistance of 4–6 MΩ. Light-evoked inhibitory postsynaptic currents (leIPSCs) were recorded in the voltage-clamp configuration using an intracellular solution containing the following (in mM): 120 D-gluconic acid, 100 CsOH, 1 TEA-OH, 10 Hepes, 6 NaCl, 16 BAPTA, 0.1 QX314-Cl, 1 $CaCl_2$, 10 potassium phosphocreatine, 4 Mg-ATP, 0.4 Na-GTP, pH adjusted to 7.35 with CsOH with a final osmolarity of 295–305 mOsm. For the current clamp experiments described in **Figure 2**, the following intracellular solution was used (in mM): 135 $KMeSO_4$, 3 NaCl, 1 $MgCl_2$, 10 potassium phosphocreatine, 10 Hepes, 4 Mg-ATP, 0.4 Na-ATP pH adjusted to 7.35 with KOH with a final osmolarity of 295-305 mOsm.

The brief (1–2 ms long) flashes of blue light used to evoke leIPSCs were provided by triggering either a lambda DG-4 device (Sutter Instruments), or a 470-nm wavelength LED (Thorlabs) coupled to the slice chamber via the epi-fluorescence pathway of the microscope. Recruitment of axons was observed up to full-field powers of 11.5 mW, with a threshold of around 0.25 mW.

All electrophysiological recordings were performed with a double EPC-10 amplifier (Heka Elektronik) run by Patchmaster (Heka). Sampling frequency was 40 kHz. Data were filtered at 3 kHz. All data were analyzed using Igor (Wavemetrics, Lake Oswego, OR) and with routines developed in-house. Statistical comparisons were performed using the Mann-Whitney *U* test, the Wilcoxon signed rank test for paired sets of data and in the case of the data of **Figure 3i–j**, a paired *t* test. Statistical significance was set at 0.05. Results are given as mean ± s.e.m.

Anesthesia and surgery. 11 adult male C57Bl/6J BAC *Glyt2-eGFP* mice (20–30 g) were used for the experiments. Surgeries and experiments were done under

doi:10.1038/nn.3951

ketamine/xylazine anesthesia. Initially, mice received intraperitoneal injection of ketamine (111 mg per kg) and xylazine (4.3 mg per kg). For the maintenance of the anesthesia, intramuscular injection of ketamine/xylazine was given every 30–50 min during the entire duration of the experiments.

***In vivo* juxtacellular recording and labeling, local field potential (LFP) recording.** Bipolar LFP electrodes (FHC, resistance ~1 MΩ) were placed into the frontal cortex of mice (AP: +1.7 mm, L: −0.8 mm from Bregma). The recorded signal was amplified, band-pass filtered from 0.16 Hz to 5 kHz and from 100 Hz to 5 kHz to record the fast multiunit activity (Supertech BioAmp, Supertech) and digitized at 20 kHz (micro 1401 mkii, CED). Concentric bipolar stimulating electrodes were inserted into the IL (Bregma AP, −1.5 mm; ML, 2 mm; DV, −3.2 mm tilted at 20 degrees, electrode separation 0.8 mm). PnO single unit activity was recorded by glass microelectrodes (*in vivo* impedance of 20–40 MΩ) pulled from borosilicate glass capillaries (1.5-mm outer diameter, 0.75- or 0.86-mm inner diameter, Sutter Instrument or WPI) and filled with 0.5 M potassium acetate and 2% neurobiotin (wt/vol, Vector Laboratories). Electrodes were lowered by a piezoelectric microdrive (Burleigh 6000 ULN or ISS 8200, EXFO) into the PnO (Bregma AP, −4.4 mm; ML, 0.8–1.0 mm; DV, −3.8–4.8 mm). Neuronal signals were amplified by a DC amplifier (Axoclamp 2B, Axon Instruments/Molecular Devices, Sunnyvale, CA, USA), further amplified and filtered between 0.16 Hz and 5 kHz by a signal conditioner (LinearAmp, Supertech). Neuronal signals were recorded by Spike2 5.0 (CED). Juxtacellular labeling of the recorded neurons was done as described previously[44]. Following perfusion, coronal sections (50 µm) were cut from the PnO and the neurons were visualized by Cy3-conjugated streptavidin (1:2,000, Jackson). *Glyt2-eGFP* positivity was determined by confocal microscope. The neurons were then developed using ABC and DAB-Ni, and the sections containing the labeled neurons were dehydrated and embedded in Durcupan. The dendritic trees of the labeled neurons were reconstructed using Neurolucida 5.2 software (MBF Bioscience).

Analysis. To determine the action potential clusters of the PnO cells, we used a built-in script of Spike2 7.0 (CED) software. We identified clusters by separating the two peaks at the minimum of the bimodal interspike interval histograms (ISI). Cortical population activity was dominated by the cortical slow oscillation (quasi-periodic alternation of active, 'UP', and inactive, 'DOWN', states) in the anesthetized animals. We determined the phase of each action potential relative to this oscillation for the recorded neurons as described previously[45]. Briefly, the envelope of the cortical multiunit trace (MUA envelope) was low-pass filtered at 4 Hz using a zero phase-shift finite impulse response filter; the Hilbert-transform of the filtered and z-scored MUA envelope was calculated and the phase was determined by taking the angle of the complex 'analytic signal'. The prime advantage of this method is that it estimates the phase of any quasi-rhythmic signal in a temporally refined manner, defining a time series that quantifies the 'instantaneous phase' of the ongoing oscillation[46]. The circular mean angle was calculated for each recorded neuron[47] and the inter-quartile range was determined as ±25 percentile around the circular mean.

***In vivo* optogenetics.** 4 weeks after transfection of PnO cells with either a ChR2-eYFP or eYFP virus, *Glyt2-Cre* animals were anesthetized with ketamine-xylazine (100 and 5 mg per kg) and placed in a stereotactic frame. Once exposed, the skull was cleaned with H_2O_2 and covered with a layer of Super Bond C&B (Morita). A craniotomy was performed over the right hemisphere and an optic fiber (200 µm, 0.22 NA) housed inside a connectorized implant (M3, Doric Lenses) was lowered over the caudal thalamic central lateral nucleus (Bregma −2.0 AP, +0.8 ML, −2.8 DV). The craniotomy was covered with a drop of warm agarose gel (2%), and the implant was secured with dental acrylic (Pi-Ku-Plast HP 36, Bredent). The skin was stitched at the rear and front of the implant and the animal was allowed to recover on a heating pad. Mice were allowed to recover for at least 5 d before testing.

The following custom optical system was used for fiber optic light delivery in freely moving mice: the beam generated by a 473-nm DPSS laser (LRS-0473-PFM-00100-03, Laserglow Technologies) was passed through an acousto-optic tunable filter (AOTFnC-400.650-TN, AA Opto-Electronic) controlled by a multi digital synthesizer (MDS4C-D66-22-74.158-RS), allowing accurate and silent light pulse generation. The first order beam exiting the AOTF was bounced on mirrors and directed into the core of a fiber optic patchcord (200 µm, 0.37 NA) through a custom table-top rotary joint (Doric Lenses). The patchcord (1.6 m) was connected to the mouse and allowed to rotate passively. With adequate beam alignment, rotations induced power fluctuations of less than 5% at the fiber output. The power density measured at the output of the delivery fiber was 318 mW mm^{-2} for 200-µm-diameter optic fiber (behavioral experiments) and 1,272.73 mW mm^{-2} for the 100-µm-diameter fiber (electrophysiological experiments).

For motility tests, each mouse was tested in six sessions, with a maximum of one session per day. During each session, mice were allowed to move freely on an open white platform while being filmed continuously via a CCD camera (Guppy Pro, Allied Vision) and exposed to 10-s trains of 5-ms light pulses delivered at 30 Hz every minute for 15 min. Photostimulation trains were signaled on the video recording by an infrared LED. All aspects of the experiment (photostimulation waveform generation, MDS and LED control, video recording) were controlled using LabVIEW (National Instruments). Movies were analyzed off-line with Ethovision (Noldus Technology) to extract animal trajectories and speed profiles. Statistical comparisons were performed using the Mann-Whitney *U* test or the Wilcoxon signed rank test for paired sets of data.

To record cortical LFP signals from freely moving animals we implanted bipolar electrodes into the frontal cortex. We used screws placed above the cerebellum as a reference and ground. Both the LFP recording electrodes and the reference and ground electrodes were soldered to an 18 Position Dual Row Male Nano-Miniature Connector (A79014-001, Omnetics Connector). The optic fiber was lowered into the intralaminar thalamus. The whole implant was fixed with dental acrylic and surrounded with copper grid. For LFP measurements, 30-s-long stimulations were used (3–5 stimulations per d with 5–10 min between them). To record the LFP signals, we used a 128-channel amplifier (Amplipex). For wavelet generation, we used homemade MatLab scripts.

Statistics. Statistical comparisons were performed using the Mann-Whitney *U* test, the Wilcoxon signed rank test for paired sets of data and in the case of the data of **Figure 3i–j**, a paired *t* test. Statistical significance was set at 0.05 but the exact values are reported. Results are given as mean ± s.e.m. No statistical methods were used to predetermine sample sizes, but our sample sizes are similar to those reported in previous publications[21,27,35]. Equal variances were not formally tested. For the behavior experiments, mice were randomly assigned to hChR2.eYFP and eYFP groups. For anatomical, *in vitro* and *in vivo* physiological experiments, no exclusion criteria was applied for the initial selection and data were collected randomly. All physiology data were processed by automated software, eliminating the possibility of biases in data processing. The experimenters were not blind to the conditions of the animals.

A **Supplementary Methods Checklist** is available.

42. Ollion, J., Cochennec, J., Loll, F., Escudé, C. & Boudier, T. TANGO: a generic tool for high-throughput 3D image analysis for studying nuclear organization. *Bioinformatics* **29**, 1840–1841 (2013).
43. Somogyi, P., Hodgson, A.J., Chubb, I.W., Penke, B. & Erdei, A. Antisera to gamma-aminobutyric acid. II. Immunocytochemical application to the central nervous system. *J. Histochem. Cytochem.* **33**, 240–248 (1985).
44. Pinault, D. A novel single-cell staining procedure performed *in vivo* under electrophysiological control: morpho-functional features of juxtacellularly labeled thalamic cells and other central neurons with biocytin or Neurobiotin. *J. Neurosci. Methods* **65**, 113–136 (1996).
45. Slézia, A., Hangya, B., Ulbert, I. & Acsády, L. Phase advancement and nucleus-specific timing of thalamocortical activity during slow cortical oscillation. *J. Neurosci.* **31**, 607–617 (2011).
46. Hurtado, J.M., Rubchinsky, L.L. & Sigvardt, K.A. Statistical method for detection of phase-locking episodes in neural oscillations. *J. Neurophysiol.* **91**, 1883–1898 (2004).
47. Fisher, N. *Statistical Analysis of Circular Data* (Cambridge University Press, 1993).